Coincidence Measurements of Ne^+–Ne Collisions*

QUENTIN C. KESSEL,† MICHAEL P. MCCAUGHEY, AND EDGAR EVERHART
Physics Department, The University of Connecticut, Storrs, Connecticut
(Received 29 August 1966)

A study is made of single collisions of keV-energy Ne ions with Ne atoms wherein both particles scattered from the same encounter are detected in coincidence. The charge states m of the scattered incident particle and n of the recoiling target particle are determined. The relative probability of the (m,n) reaction and the associated inelastic energy loss are measured as to their dependence upon the scattering angles and the incident energy T_0. The statistical model proposed by Everhart and Kessel is used to analyze the data. At the higher energies (T_0 from 150 to 400 keV), a double structure is found in the values of inelastic energy loss. This structure is attributed to a K-shell vacancy found with low probability in some of the neon particles after the collision. The expected Auger electrons are detected and found to have 750-eV energy.

1. INTRODUCTION

THE present study of large-angle Ne^+–Ne collisions is parallel to our recent study of Ar^+–Ar collisions. The experiment follows the same pattern,[1] and the results are analyzed according to the same statistical model.[2] In the present Ne^+–Ne study, evidence is found (at high energies) for a K-shell vacancy induced by the collision.[3] The experiment shows[3] a double-peaked structure in the inelastic energies and emitted electrons of 750 eV which are thought to be KLL Auger electrons.

Coincidence measurements of Ne^+–Ne at 50 keV have been reported by Afrosimov, Gordeev, Panov, and Fedorenko,[4] and these will be compared where there are data in common. Studies of various other aspects of large-angle Ne^+–Ne collisions at keV energies (not using coincidence methods) include those of Fuls *et al.*,[5] Jones *et al.*,[6] Ziemba *et al.*,[7] Flinchbaugh,[8] and Lane and Everhart.[9]

The reaction under study is

$$Ne^+ + Ne \rightarrow Ne^{+m} + Ne^{+n} + (m+n-1)e. \qquad (1)$$

The incident ion is scattered to angle θ with charge $+m$, and the recoil target particle is found at angle ϕ with charge $+n$. The incident-ion energy T_0 ranges from 6 to 400 keV, and the angle θ is varied from 8° to 40°. The relative probability $\bar{p}_{mn}$ and the inelastic energy loss $\bar{Q}_{mn}$ are measured for reactions in which m and n are both specified.

2. PROCEDURE

The theory of the measurement, the apparatus, and the procedure have been described.[1] A simultaneous measurement is made of the angles θ and ϕ. The inelastic energy Q is then found[1] using

$$Q = T_0\{1 - [\sin^2(\beta-\theta) + \gamma \sin^2\theta]/\sin^2\beta\}, \qquad (2)$$

where T_0 is the incident energy, $\beta = \theta + \phi$, and the mass ratio γ is unity. A possible complication in the value of γ due to the two isotopes of neon is avoided by using isotopically pure neon (99.7% mass 20). When the detectors are set to study the (m,n) event, the angles θ and β are used to find $\bar{Q}_{mn}$, and the number of such events determines $\bar{p}_{mn}$, the relative probability of the (m,n) event. Here the normalization is such that $\sum_{m,n} \bar{p}_{mn} = 1$.

At high energies, where structure is found in the $\bar{Q}_{mn}$ values, fast electrons are detected in this study. For such measurements one detector is set at 115° and electron energies are measured. The electron counting is not done in coincidence with the scattered ions. In our preliminary measurement[3] using an electron energy analyzer, there was an error caused when stray magnetic fields were not properly compensated. The 650-eV energy previously reported is here corrected to 750±20 eV.

3. DATA AND DISCUSSION

A. Q-Values

Table I gives values of $\bar{Q}_{mn}$ for several data sets wherein T_0 and θ are held constant. Here $\bar{Q}_{TT} \equiv \bar{Q}$ refers to an over-all average inelastic energy where particles of all charge states are counted. A few values of $\bar{Q}_{mn}$, taken at 50 keV in the angular range 4°–40°, have been

* Research sponsored by the Air Force Office of Scientific Research, Office of Aerospace Research, U. S. Air Force, under AFOSR Grant No. AF-AFOSR-805-65.

† Now with Research Division, High Voltage Engineering Corporation, Burlington, Massachusetts.

[1] Q. C. Kessel and E. Everhart, Phys. Rev. **146**, 16 (1966).

[2] E. Everhart and Q. C. Kessel, Phys. Rev. **146**, 27 (1966).

[3] Q. C. Kessel, M. P. McCaughey, and E. Everhart, Phys. Rev. Letters **16**, 1189 (1966); **17**, 1170 (1966).

[4] V. V. Afrosimov, Yu. S. Gordeev, M. N. Panov, and N. V. Fedorenko, Zh. Tekhn. Fiz. **36**, 123 (1966). [English transl.: Soviet. Phys.—Tech. Phys. **11**, 89 (1966)].

[5] Ionization probabilities and differential cross sections: N. E. Fuls, P. R. Jones, F. P. Ziemba, and E. Everhart, Phys. Rev. **107**, 704 (1957).

[6] Ionization probabilities, inelastic processes, and resonant electron capture: P. R. Jones, F. P. Ziemba, H. A. Moses, and E. Everhart, Phys. Rev. **113**, 182 (1959); P. R. Jones, P. Costigan, and G. Van Dyk, *ibid.* **129**, 211 (1963); P. R. Jones, N. W. Eddy, H. P. Gilman, A. K. Jhaveri, and G. Van Dyk, *ibid.* **147**, 76 (1966); P. R. Jones, T. L. Batra, and H. A. Ranga, Phys. Rev. Letters, **17**, 281 (1966).

[7] Resonant electron capture: F. P. Ziemba, G. J. Lockwood, G. H. Morgan, and E. Everhart, Phys. Rev. **118**, 1552 (1960). See Figs. 8(a), 8(b), and 10(a).

[8] Inelastic energy losses: D. E. Flinchbaugh, J. Chem. Phys. **43**, 910 (1965).

[9] Intermolecular Ne^+–Ne potential energy: G. Lane and E. Everhart, Phys. Rev. **120**, 2064 (1960).

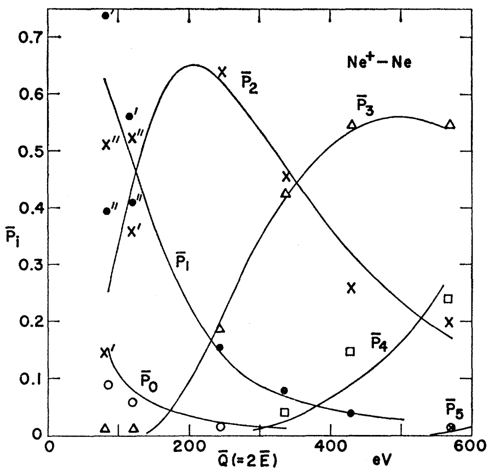

FIG. 1. Average ionization probabilities $\bar{P}_i$ are plotted versus average inelastic energy $\bar{Q}$ for several data sets. The two lowest data sets have primes to refer to the scattered incident particle and double primes to indicate recoil target particle. The solid lines are computed through the use of a statistical model as discussed in text.

published by Afrosimov *et al.*[4] These agree fairly well with the 50-keV, 10° entries in Table I.

Table II gives values of $\bar{p}_{mn}$ for several data sets. Upon adding the columns of Table II one finds $\bar{P}_i' = \sum_n \bar{p}_{in}$, which is the probability of finding charge state i among the scattered particles. Adding the rows gives $\bar{P}_i'' = \sum_m \bar{p}_{mi}$, the corresponding quantity for the recoil particles. At the lowest two energies, there were systematic differences between $\bar{P}_i'$ and $\bar{P}_i''$, as indicated by the single-primed (scattered) and double-primed (recoil) points plotted versus $\bar{Q}$ in Fig. 1. Evidently, the scattered and recoil particles do not have the same average charge state after the collision at low energies.[10] At higher energies, however, $\bar{P}_i'$ and $\bar{P}_i''$ were found to be equal within data scatter and their average, termed $\bar{P}_i$, is plotted in Fig. 1. The solid lines in this figure represent a fit to the data which is achieved using a statistical model as described in Sec. 4 below.

Values of $\bar{Q}_{mn}$ are plotted versus $\bar{Q}$ in Fig. 2 and it is significant that $\bar{Q}_{mn}$ is not independent of $\bar{Q}$. Thus $\bar{Q}_{22}$ increases uniformly from 170 to 305 eV, depending on the violence of the collision. A similar behavior is seen in the Ar^+–Ar data.[1] This continuous variation of $\bar{Q}_{mn}$ is not explained by a recently proposed concept of

TABLE I. The inelastic energy $\bar{Q}_{mn}$ is given for Ne^+–Ne reactions where charge states m and n after collision are specified. The notation T,T refers to an overall average. Thus $\bar{Q}_{TT} \equiv \bar{Q}$.

T_0(keV),θ	m,n	$\bar{Q}_{mn}$ (eV)	m,n	$\bar{Q}_{mn}$ (eV)
6.4, 10°	T,T	85±5	1,1	70±5
	0,1	60±15	1,2	100±10
	1,0	45±20		
6.4, 40°	T,T	130±10		
12, 10°	T,T	120±10	2,1	120±5
	1,1	90±5	2,2	170±10
12, 40°	T,T	230±10		
25, 10°	T,T	245±10	2,2	230±10
	1,2	185±10	2,3	290±10
25, 40°	T,T	325±15		
50, 10°	T,T	335±10	2,3	345±15
	2,1	195±15	3,3	415±15
	2,2	260±15		
50, 40°	T,T	450±20		
100, 10°	T,T	440±15	2,4	510±40
	2,2	305±25	3,3	475±25
	2,3	390±25	3,4	575±25
100, 40°	T,T	550±100		
150, 10°	T,T	520±30	3,4	610±35
	3,3	510±40	4,4	770±45
200, 8°	T,T[a]	570±20	5,3[a]	710±80
	5,4[a]	770±100	5,3[b]	1550±100
	5,4[b]	1630±100	4,3[a]	670±50
300, 8°	T,T[c]	680±80		
400, 8°	T,T[c]	830±60		

[a] Data correspond to first peak.
[b] Data correspond to second peak.
[c] Data correspond to first peak, but with Ne^{++} incident.

TABLE II. The relative probability $\bar{p}_{mn}$ of the (m,n) event is given for Ne^+–Ne collisions. Other values can be read from Fig. 5 for data sets not given here.

6.4 keV, 10° ($\bar{m}=1.09$, $\bar{n}=1{,}45$. total events=547)				
$m=$	0	1	2	
$n=0$	...	0.050	0.029	
$n=1$	0.026	0.271	0.097	
$n=2$	0.068	0.413	0.024	
12 keV, 10° ($\bar{m}=1.32$, $\bar{n}=1.49$, total events=871)				
$m=$	0	1	2	3
$n=0$	...	0.018	0.031	0.007
$n=1$	0.008	0.209	0.187	0.005
$n=2$	0.051	0.330	0.142	0.000
$n=3$	0.003	0.008	0.000	0.000
25 keV, 10° ($\bar{m}=1.98$, $\bar{n}=2.03$, total events=4583)				
$m=$	0	1	2	3
$n=0$	...	0.000	0.018	0.002
$n=1$	0.001	0.024	0.084	0.022
$n=2$	0.005	0.117	0.409	0.109
$n=3$	0.002	0.037	0.128	0.034
50 keV, 10° ($\bar{m}=2.42$, $\bar{n}=2.43$, total events=57,867)				
$m=$	1	2	3	4
$n=1$	0.005	0.034	0.031	0.006
$n=2$	0.036	0.208	0.189	0.021
$n=3$	0.037	0.197	0.183	0.015
$n=4$	0.006	0.019	0.013	0.001

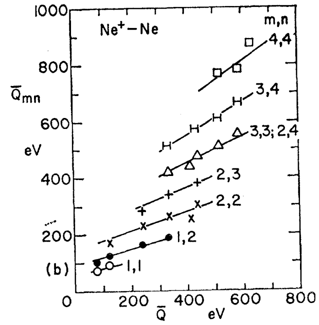

FIG. 2. Values of $\bar{Q}_{mn}$ are plotted versus $\bar{Q}$ for several (m,n) values.

[10] The region at low energies where $\bar{P}_i'$ and $\bar{P}_i''$ differ is not investigated completely. The two data sets in question refer to 6.4 keV, 10° and to 12 keV, 10°. Other scattering angles and energies, even where $\bar{Q}$ is the same, might well show a different behavior in this low energy region.

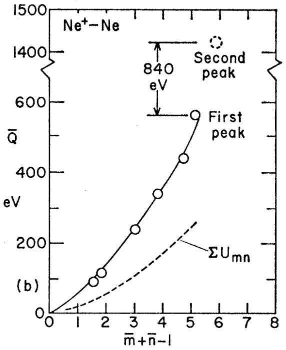

FIG. 3. Average inelastic energy $\bar{Q}$ for each data set is plotted versus $\bar{m}+\bar{n}-1$, the average number of electrons lost in that data set. The dashed line, labeled $\sum U_{mn}$, shows that portion of the inelastic energy accounted for by spectroscopic ionization energies.

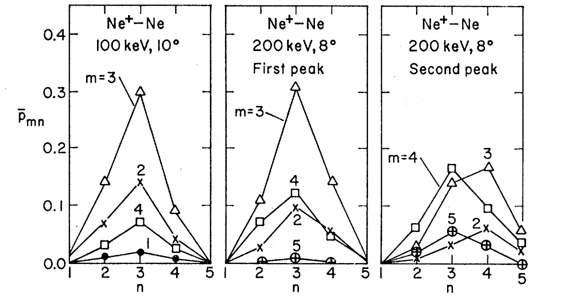

FIG. 5. Values of the probability $\bar{p}_{mn}$ of the (m,n) event are plotted versus n with m as a parameter for three data sets.

characteristic excess energy losses,[4] but is consistent with our statistical model.[2]

The solid line in Fig. 3 shows $\bar{Q}$ plotted versus average values $\bar{m}+\bar{n}-1$ of the number of electrons lost in the collison. The dashed line in that figure indicates that portion of $\bar{Q}$ which is accounted for by spectroscopic ionization energies, $\sum U_{mn}$. The remainder, about 50% of $\bar{Q}$, is evidently due to excess kinetic energy of the emitted electrons and residual excitation.

The approximate distance of closest approach R_0 is readily calculated,[11] and Fig. 4 shows $\bar{Q}$ plotted versus R_0. Although $\bar{Q}$ depends in large measure on R_0, it is seen that there is a velocity dependence as well. Thus the data for each energy do not lie on the same line as the data for adjacent energies. Here the data above 200 keV are obtained with the Ne++–Ne collision.

B. Correlations

At the higher energies, $T_0 \geqslant 25$ keV, the values of m and n are generally uncorrelated in the sense already described.[1] This is illustrated by the 100-keV, 10° data in Fig. 5(a) and the 200-keV, 8° (first peak) data in Fig. 5(b). These curves of $\bar{p}_{mn}$ plotted versus n for each value of m all have the same shape. This empirical result and the related equation

$$\bar{p}_{mn}=\bar{P}_m\bar{P}_n \tag{3}$$

are consistent with the statistical model of these collisions.[2] Figure 5(c) shows a special case where there is correlation. Here the $\bar{p}_{mn}$ curves do not all have the same shape and Eq. (3) does not apply. This condition is related to a structure found in the Q values and is discussed in Sec. 5 below.

C. Linewidths

There is a natural distribution to the inelastic energies associated with each data set. This can be determined, approximately, from the data, starting from a plot of coincidence counts versus β and allowing for instrumental effects following procedures already described.[1] This natural width δQ^N, defined as the half-width at $1/e$ height of a fitted Gaussian curve, has been determined as a function $\bar{Q}$ for the present Ne+–Ne data. These measured linewidths can be obtained indirectly

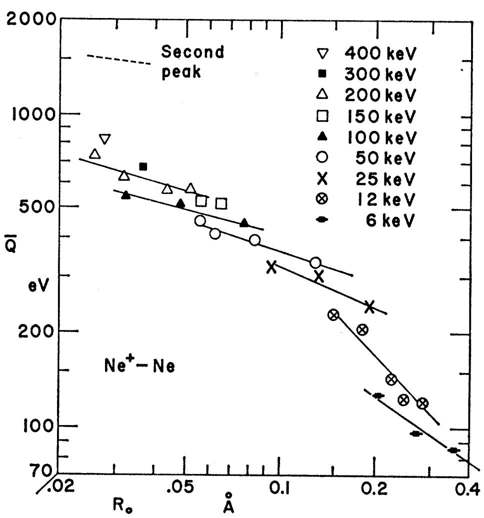

FIG. 4. The average inelastic energy $\bar{Q}$ is plotted versus R_0, the distance of closest approach. The data taken at each energy lie on a separate line.

[11] E. Everhart, G. Stone, and R. J. Carbone, Phys. Rev. **99**, 1287 (1955). A FORTRAN program for this calculation is available on request to the present authors.

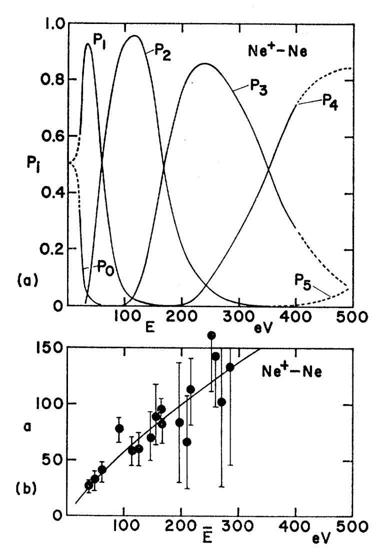

FIG. 6. (a) "Unsquashed" or intrinsic values of ionization probability P_i are plotted versus the energy E received by a neon atom. These curves are obtatned through the use of a statistical model. (b) The half-width a (at $1/e$ height) of the distribution-in-E is plotted versus average energy $\bar{E}$. The solid line shows values required to fit the data of Fig. 1 through the use of a statistical model. The data points are derived from measured line widths.

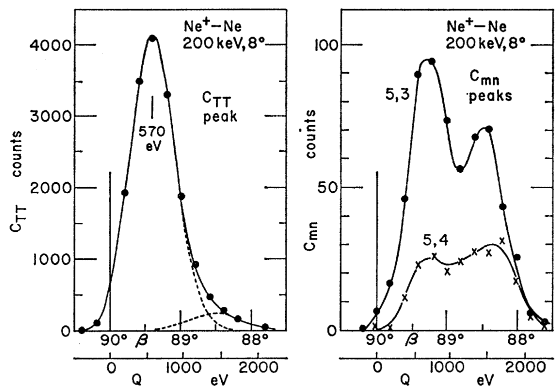

FIG. 7. (a) For Ne⁺–Ne collision at 200 keV, 8°, the number of C_{TT} coincidence counts is plotted versus the angular separation β of the two detectors. In taking this (T,T) peak all particles are counted, irrespective of their charge state. (b) Here the coincidence counts of the (5,3) and (5,4) reactions are plotted versus β.

from the points in Fig. 6(b), where a, which equals $0.7\delta Q^N$, is plotted versus $\bar{E}$, which equals $\frac{1}{2}\bar{Q}$.

4. STATISTICAL MODEL

The statistical model of Everhart and Kessel[2] is applied to the present data. The model starts with the Russek-Thomas theory,[12] which postulates the existence of intrinsic ionization probabilities P_i that are functions of the inelastic energy E received by either atom. Our model postulates further that there is a Gaussian distribution to the values of E which each atom receives. The half-width a (at $1/e$ height) of this distribution is adjusted.

Working with the model as described,[2] we obtain the P_i-versus-E curves of Fig. 6(a) for Ne⁺–Ne. These curves, obtained here by working with the data, should be predictable *a priori* by the Russek-Thomas theory. These "unsquashed" or intrinsic values of $P_i(E)$, when averaged over a distribution in the E values for each data set, result in the solid curves drawn in Fig. 1. The necessary half-widths a are found empirically and are shown as the solid line in Fig. 6(b). This solid line is reasonably consistent with the data points in this figure, which are derived from measured linewidths.

The fit shown in Fig. 1 is achieved through a systematic iterative process[2] which yields unique answers; i.e., significantly different $a(\bar{E})$ or $P_i(E)$ curves would not fit the data as well. The criteria for best fit are twofold: (1) The predicted $\bar{P}_i(\bar{Q})$ curves (shown solid) on Fig. 1 must lie fairly close to the data points. (2) The predicted $\bar{Q}_{mn}$ values should lie fairly close to the measured values. Table III compares the data and the model for three data sets. There is encouraging over-all agreement. The statistical model used here is considered to be a useful semi-empirical description. It is recognized that

TABLE III. Comparison of measured and predicted values of $\bar{P}_i$, $\bar{p}_{mn}$, and $\bar{Q}_{mn}$.
Data set A: $T_0 = 25$ keV, $\theta = 10°$, $\bar{Q} = 245 \pm 10$ eV, $a = 68$ eV;
B: $T_0 = 50$ keV, $\theta = 10°$, $\bar{Q} = 335 \pm 10$ eV, $a = 87$ eV;
C: $T_0 = 100$ keV, $\theta = 10°$, $\bar{Q} = 440 \pm 15$ eV, $a = 113$ eV.

Data set	i	$\bar{P}_i$ Data	$\bar{P}_i$ Model	m,n	$\bar{p}_{mn}$ Data	$\bar{p}_{mn}$ Model	$\bar{Q}_{mn}$ (eV) Data	$\bar{Q}_{mn}$ (eV) Model
A	0	0.014	0.023	1,2	0.117	0.188	185±10	165
	1	0.158	0.142	2,2	0.409	0.386	230±10	256
	2	0.640	0.622	2,3	0.128	0.131	290±10	290
	3	0.186	0.210	1,1	0.024	0.020		
				1,3	0.037	0.030		
				3,3	0.034	0.044		
B	0	0.000	0.013	2,1	0.034	0.034	195±15	183
	1	0.080	0.072	2,2	0.208	0.225	260±15	270
	2	0.456	0.474	2,3	0.197	0.197	345±15	335
	3	0.424	0.415	3,3	0.183	0.172	415±15	400
	4	0.040	0.026	3,1	0.031	0.030		
				2,4	0.019	0.012		
C	1	0.039	0.040	2,2	0.070	0.104	305±25	286
	2	0.260	0.322	2,3	0.137	0.172	390±25	371
	3	0.545	0.534	2,4	0.039	0.031	510±40	443
	4	0.148	0.096	3,3	0.305	0.285	475±25	456
	5	0.007	0.000	3,4	0.081	0.051	575±25	528
				4,4	0.019	0.009		
				3,1	0.020	0.022		

the phenomena described by these smoothed curves of Figs. 1 and 6 may be an average over a large number of unresolved discrete reactions.

5. Q STRUCTURE

In Figs. 3 and 4, discontinuities are seen at high energies, which indicate a double structure in the Q values. In measurements taken at 200 keV, 8°, a plot of coincidence counts C_{TT} versus the relative angle β of the recoil-particle detector shows the asymmetric shape pictured in Fig. 7(a). The peak corresponds to a Q value of 570 eV, but there is a suggestion of a weak high-energy component. This suspected second peak is resolved in Fig. 7(b), which shows the corresponding plot for the (5,3) and (5,4) combinations. Similar plots for other (m,n) values do not show the structure as well.

A tentative interpretation of this structure may be given along lines already indicated.[2,3,13] Immediately after the collision, a neon atom may be in either of two states: state A, corresponding to an L-shell excitation, or state B, where there is also a K-shell vacancy. Most events are AA, and this corresponds to the predominant first peak. State B is rare and the weak second peak suggested in Fig. 7(a) corresponds to the case AB (or BA). The case BB is so rare that the third peak is not seen.

The charge states associated with the two peaks are shown in Figs. 5(b) and 5(c), respectively. It is seen that charge state +5 is unlikely in the first peak, but is fairly common in the second peak. Following the above description, one would surmise that state +5 is a common consequence of state B but rare for state A. For this reason, the rare second peak should be more easily

[12] A. Russek and M. T. Thomas, Phys. Rev. **109**, 2015 (1958); **114**, 158 (1959); J. B. Bulman and A. Russek, *ibid.* **122**, 506 (1961); A. Russek, *ibid.* **132**, 246 (1963); A. Russek and J. A. Meli (to be published).

[13] Q. C. Kessel, A. Russek, and E. Everhart, Phys. Rev. Letters **14**, 484 (1965).

observed in cases where one of the particles is 5× ionized. Thus the (5,3) and (5,4) cases pictured in Fig. 7(b) show both peaks. Equations (21)–(23) of Ref. 2 (with a small value of α as defined in that paper) can be applied here to make this discussion quantitative.

The statistical model[2,13] predicts that charge states m and n should be uncorrelated for events contributing to the first peak, but should be correlated in a particular way for the second peak. This may be seen on comparing Fig. 5(b) with Fig. 5(c). These bear a strong resemblance to Figs. 1(a) and 2(b) of Ref. 13, which show corresponding plots for the first and second peaks in Ar^+–Ar structure.

A "promotion" mechanism has been suggested by Fano and Lichten[14] to account for an inner-shell vacancy in Ar^+–Ar collisions, and Rudd *et al.*[15] have recently detected *LMM* Auger electrons in such collisions.

In the present Ne^+–Ne study it was expected that, similarly, there might be a *KLL* Auger electron observable which arises from the postulated *K*-shell vacancy. We have seen such electrons and find their energy to be 750±20 eV. The electron specta were taken in a noncoincidence measurement at several energies between 150 and 400 keV, as described in Ref. 3.

[14] U. Fano and W. Lichten, Phys. Rev. Letters, **14**, 627 (1965).
[15] M. E. Rudd, T. Jorgensen, and D. J. Volz, Phys. Rev. **151**, 28 (1966).

ACKNOWLEDGMENTS

Professor M. Eugene Rudd has generously shared with us his experience and techniques for electron spectra measurement.

We thank Miss Marianne Melnick and Emile Knystautas, who helped reduce the data. The computational part of this work was carried out in the Computer Center of the University of Connecticut, which is supported in part by Grant GP-1819 of the National Science Foundation.

PHYSICAL REVIEW VOLUME 153, NUMBER 1 5 JANUARY 1967

Reduced-Density-Matrix Theory: The 2-Matrix of Four-Electron Systems*

GENE P. BARNETT† AND HARRISON SHULL
Chemistry Department, Indiana University, Bloomington, Indiana
(Received 6 June 1966)

The theory of reduced density matrices for polyelectronic systems is formulated in a manner such that the reduced density matrix of any order p is characterized by a coefficient matrix. This matrix of coefficients, resulting from expressing the polyelectronic wave function in the appropriate bilinear form, is sufficient to allow one to find the eigenvalues and the transformation to natural form. This formalism is a generalization of the work of Löwdin and Shull on the natural orbitals of two-electron systems. The second-order reduced density matrix, the 2-matrix, is obtained exactly from the approximate solutions Ψ of the Schrödinger equation for the Be-atom functions of Weiss, Watson, and Boys, and the LiH function of Ebbing. The important eigenfunctions and complete eigenvalue spectra of the integral operator $\Gamma^{(2)}$, which has the 2-matrix as kernel, are reported here. The degeneracies of the eigenvalue spectra of $\Gamma^{(2)}$ and the properties of the natural geminals, the eigenfunctions of $\Gamma^{(2)}$, are discussed in detail. The multiplicities 1, 2, 3, 4, and 6 are the only nonaccidental degeneracies that can occur in the 4-electron problem when the one-electron basis of Ψ is considered in symmetry-adapted spin-orbital form. The natural geminals can always be obtained in symmetry-adapted form and can be completely described by a set of numbers (λ, s, m_s, m_l, . . .), eigenvalues for the operators $\Gamma^{(2)}$, S^2, S_z, L_z, . . ., respectively. The identity of the eigenvalue spectra and the equivalence of the two operators $\Gamma^{(p)}$ and $\Gamma^{(N-p)}$ are demonstrated in the case where the one-electron basis of Ψ is finite. The natural expansion of Ψ is defined as the expansion in eigenfunctions of $\Gamma^{(p)}$ and $\Gamma^{(N-p)}$. In the case $2p=N$, the phase of the two sets of eigenfunctions can be chosen as equal and the signs of the natural expansion coefficients are uniquely determined by the function Ψ.

I. INTRODUCTION

DENSITY-MATRIX analysis of two-electron wave functions has yielded many useful and interesting results.[1] The rapid convergence and simplicity of form of the natural expansion,[2,3] the utility of natural orbitals in comparing approximate wave functions and studying chemical bonding,[4–7] and some special solutions of the N-representability problem[8] are examples. Considerable

* Supported by grants from the National Science Foundation and the U. S. Air Force Office of Scientific Research.
† Present address: Theoretical Physics Group, Lockheed Research Laboratory, Lockheed Missiles & Space Company, Palo Alto, California.
[1] P.-O. Löwdin and H. Shull, Phys. Rev. **101**, 1730 (1956).
[2] P.-O. Löwdin, Phys. Rev. **97**, 1474 (1955).
[3] H. Shull and P.-O. Löwdin, J. Chem. Phys. **30**, 617 (1959).
[4] H. Shull, J. Chem. Phys. **30**, 1405 (1959).
[5] S. Hagstrom and H. Shull, Rev. Mod. Phys. **35**, 624 (1963).
[6] H. Shull and F. P. Prosser, J. Chem. Phys. **40**, 233 (1964).
[7] D. D. Ebbing and R. C. Henderson, J. Chem. Phys. **40**, 2225 (1965).
[8] C. E. Reid and Y. Öhrn, Rev. Mod. Phys. **35**, 445 (1963).